

Article

Design of an Optimum Compact EGR Cooler in a Heavy-Duty Diesel Engine towards Meeting Euro 7 Emission Regulations

Emrah Gumus *  and Murat Otkur 

College of Engineering and Technology, American University of the Middle East, Egaila 54200, Kuwait; murat.otkur@aum.edu.kw

* Correspondence: emrah.gumus@aum.edu.kw

Abstract: Exhaust gas recirculation (EGR) has been an efficient emission treatment strategy employed in internal combustion engines (ICEs) to cope with NO_x emission limits since the introduction of Euro 4 regulations for heavy-duty commercial vehicles. A portion of the exhaust gas is fed back into the intake port, replacing O₂ in the fresh air with inert CO₂ from the exhaust gas, resulting in a reduction in the combustion temperature and, hence, a reduction in NO_x emissions. Considering the high exhaust temperature, this process increases the charge mixture temperature and degrades the volumetric efficiency of the engine. EGR coolers have been introduced as vital parts of EGR exhaust treatment systems with the aim of reducing the intake port temperature to increase volumetric efficiency and further reduce combustion temperatures. EGR coolers are heat exchangers (HXs) that generally employ engine coolant to reduce the EGR temperature with effectiveness values around 0.7–0.85 and downgrade with engine usage owing to soot deposition. Increasing the effectiveness of the EGR cooler has a positive effect on engine volumetric efficiency and reduces NO_x, particulate matter (PM), and fuel consumption. The current study involved the design of a microchannel HX for a 500 PS heavy-duty Euro 6 diesel engine EGR cooler. The mechanical and thermal-hydraulic design calculations of the proposed HX were performed using Mathematica software. The optimum HX dimensions for the required boundary conditions were determined, and the performance of the EGR cooler was analyzed for the current and proposed options. Furthermore, Diesel-RK software was used to model the engine performance with NO_x, PM, CO₂ emissions, and fuel consumption predictions. The results show that the newly proposed microchannel HX design improves NO_x, PM, and specific fuel consumption by 6.75%, 11.30%, and 0.65%, respectively.

Keywords: emissions; EGR cooler; compact heat exchanger; Diesel-RK; Euro 7



check for updates

Citation: Gumus, E.; Otkur, M. Design of an Optimum Compact EGR Cooler in a Heavy-Duty Diesel Engine towards Meeting Euro 7 Emission Regulations. *Sustainability* **2023**, *15*, 12361. <https://doi.org/10.3390/su151612361>

Academic Editors: Denghui Wang and Yanqing Niu

Received: 17 July 2023

Revised: 9 August 2023

Accepted: 10 August 2023

Published: 14 August 2023



Copyright: © 2023 by the authors. Licensee MDPI, Basel, Switzerland. This article is an open access article distributed under the terms and conditions of the Creative Commons Attribution (CC BY) license (<https://creativecommons.org/licenses/by/4.0/>).

1. Introduction

The automotive industry is facing a critical challenge in terms of decreasing air pollution and mitigating the impact of greenhouse gas (GHG) emissions on the environment. To address these pressing concerns, the adoption of cleaner and more environment-friendly technologies in vehicle design has become paramount. The introduction of Euro 6 emission standards in 2013 resulted in 80% and 77% reductions in NO_x emissions for steady-state and transient engine testing conditions, respectively [1,2]. The European Commission recently proposed Euro 7 emission standards that are planned to become effective in 2025 and 2027 for passenger cars, light-duty commercial vehicles, and heavy-duty commercial vehicles [3]. Considering the light-duty and passenger-car segments, diesel vehicle NO_x emissions are limited to 60 mg/km compared to the 80 mg/km limit in the Euro 6 standards, using the same cycle as Euro 6: the Worldwide Harmonized Light Vehicles Test Cycle (WLTC). For heavy-duty vehicles, the new standard level introduces two sets of limits, 350 and 90 mg/kWh, for cold and hot engine conditions, respectively, compared with the NO_x limit of 460 mg/kWh applied in Euro 6 standards, using the same

cycle as Euro 6: the World Harmonized Transient Cycle (WHTC). Additionally, for light-duty and passenger-car segments, emission conformity for real-world driving scenarios is much stricter, such as short trips, which need to be taken into account, and reduced conformity factors. Furthermore, the worst-case scenario limits are enhanced, for example, the ambient temperature limit is increased from 35 °C to 45 °C and the maximum altitude is altered to 1800 m with respect to the 1600 m maximum in the Euro 6 regulations. The heavy-duty segment is expected to have more intention towards vehicle testing that will consider service conformity (ISC) and portable emissions measurement systems (PEMS). The particulate matter emission limit in Euro 6 standards (10 mg/kWh) was modified to 12 and 8 mg/kWh for cold and hot engine conditions, respectively. Considering these stricter limits and regulations for NO_x emissions, heavy-duty vehicle manufacturers have started to spend significant work time on engine and aftertreatment hardware development and calibration optimization.

The main enablers for NO_x emissions in diesel combustion are the high combustion temperature and the presence of N₂ and O₂ molecules in the combustion chamber. Considering the natural lean combustion strategy used in diesel engines, plenty of O₂ molecules are always present in the combustion chamber. Therefore, the primary strategy for reducing NO_x emissions is to lower the combustion temperature. Several techniques have been employed in diesel engines, such as exhaust gas recirculation (EGR), retarding injection timing, splitting the main injection, and downsizing [4]. The working principle behind the EGR strategy is to employ CO₂ inert gas to reduce the combustion temperature [5]. A portion of the exhaust gas is fed back to the intake manifold of the engine. EGR gases increase the specific heat coefficient (heat capacity) of the combustion gas mixture, causing a significant reduction in the maximum combustion temperature. Lowering the combustion temperature decreases the NO_x emissions generated [6]. However, considering the high-temperature exhaust gases caused by combustion, using the EGR strategy results in an elevated charge temperature at the intake manifold, which reduces the volumetric efficiency of the engine. Furthermore, the presence of CO₂ molecules reduces the possibility of physical interactions between the fuel and O₂ molecules, lowering the stability of combustion for the same air fuel ratio (AFR). Raouf and Abdalla investigated the effect of the EGR ratio (mass of EGR gases compared to the mass of fresh intake air) on the ignition delay and combustion duration parameters [7]. The outcome of the study showed that increasing the EGR ratio results in extended ignition delay and combustion duration for the above-mentioned reasons.

To reduce the negative aspects of using exhaust gases directly, EGR coolers were introduced with the aim of lowering the charge temperature and increasing the density of air and, hence, the O₂ content for the same boost pressure [8]. Wijeyakulasuriya et al. listed examples of cooled EGR technologies such as Toyota Motor Corporation's ESTEC 2ZR-FXE with a maximum gasoline thermal efficiency of 40% [9]. Demirkesen et al. conducted a computational fluid dynamics (CFD) study using Siemens Simcenter software and validated the results with experimental test data obtained from a heavy-duty diesel engine EGR cooler [10]. The authors were able to predict the EGR outlet temperature with a sensitivity of 1 °C and the pressure drop values with a relative error of 5%.

In the last decade, compact heat exchangers have also been employed, despite the use of conventional EGR coolers (shell-and-tube heat exchangers). Hooman and Malayeri performed an experimental study considering the use of metal foams as EGR coolers and investigated the effects of aluminum foam PPI, height, and gas velocity [11]. The results show that metal-foam exchangers with proper design lead to higher heat transfer and a reasonable pressure drop when compared to no-foam coolers. Pourrezaei et al. studied the thermal performance of metal-foam-structured EGR coolers and investigated the soot deposition mechanisms with EGR inlet and coolant temperature ranges of 250–400 °C and 25–90 °C, respectively. They concluded that the importance of thermophoresis is limited in metal-foam HXs. The main mechanisms of soot deposition were identified as impaction for larger particle diameters and diffusion for smaller soot particles [12].

Although increasing the effectiveness of the EGR cooler has significant positive effects on engine performance and lower emissions, lower EGR temperatures may result in fouling of the EGR coolers owing to the condensation of water in the exhaust gas and deposition of the PM on cold EGR-cooler HX surfaces. Hydrocarbon condensation is another significant issue in the fouling of EGR coolers. Han et al. studied the phenomenon in a self-established test setup and showed that lowering the exhaust gas outlet temperature from the EGR cooler increases hydrocarbon condensation; furthermore, at temperatures above 160 °C, there is no condensation [13]. However, increasing the exhaust gas temperature reduces the effectiveness of the EGR cooler, resulting in increased NO_x emissions. Similarly, Paz et al. investigated deposit formation and EGR cooler fouling on ribbed surfaces [14].

Combustion in diesel engines depends on multiple fuel and air parameters, and the optimization of combustion is a time- and effort-intensive process. From this perspective, various professional software packages such as GT-Power and Ricardian Wave have been developed to model the combustion process. Diesel-RK is license-free software developed in 1981–1982 by the Department of Internal Combustion Engines (Piston Engines), Bauman Moscow State Technical University, and has been used by many researchers to model and optimize diesel engines. Siddique and Reddy modeled a 5.2 kW Kirloskar-make single-cylinder diesel engine to simulate the engine output parameters such as specific fuel consumption, rate of pressure rise, heat release rate, mechanical efficiency, volumetric efficiency, and exhaust emission and validated the results with experimental data [15]. The model was used for combustion chamber optimization to improve the performance of a single-cylinder diesel engine, which resulted in a significant reduction in the development time. Abdelaal et al. modeled a single-cylinder, four-stroke, water-cooled, direct-injection diesel engine and obtained a good correlation between the experimental results considering an average relative error of 3.15%, 0.03%, 26.63%, and 3% for the parameters of brake thermal efficiency (BTE), volumetric efficiency, nitric oxide emissions index (EINO_x), and smoke emissions, respectively [16].

NO_x emission prediction plays a significant role in engine hardware selection for combustion chamber geometry and injection spray parameters. From this perspective, Kuleshov developed a NO_x prediction model named the “RK-Model” based on Zeldovich’s equations, which considers the combustion bowl geometry and injection characteristics [17]. The author compared the predicted NO_x emissions with the literature data obtained from a single-cylinder heavy-duty diesel fuel engine under seven operating conditions, and the results proved that the predicted NO_x emissions had a very good correlation with the experimental test data. Muric developed a zero-dimensional two-zone diesel emission model with EGR capability and validated the simulation results using a single-cylinder engine [18]. The model calculates rate of heat release (ROHR) with a very accurate fit (less than 0.5%), which is used as the temperature input for the NO_x model. Considering the higher amount of NO_x emissions generated, exhaust gas treatment strategies, such as EGR, have become more critical. In the absence of NO_x prediction algorithms, map-based models can be used for performance and emission analysis of internal combustion engines. From this perspective, Otkur developed an emissions and fuel consumption prediction model with altitude capability for the Rotax 912 S/ULS engine used for surveillance flight parameter optimization [19].

Traditional EGR coolers such as shell-and-tube heat exchangers have limitations in terms of size, weight, and thermal efficiency. However, microchannel heat exchangers (MHE) offer several advantages when used as EGR coolers in internal combustion engines. Their compact size and high surface-area-to-volume ratio make them easily integrated into engine systems with limited space, while their enhanced heat-transfer capabilities efficiently cool EGR gases, improve engine performance, and reduce emissions. In addition, their lightweight construction reduces their overall weight, contributing to better fuel efficiency. MHEs also generate a minimal pressure drop, maintain exhaust gas flow rates, and exhibit a rapid thermal response, thereby ensuring effective cooling even under transient conditions [20]. Despite these benefits, the widespread adoption of MHEs has been

limited, primarily because of their high manufacturing costs. The complex manufacturing process and use of specialized materials contribute to the increased production costs of MHEs compared to traditional coolers. Moreover, implementing MHEs as EGR coolers requires the addition of a second cooling circuit to cool exhaust gases before recirculation. This necessitates additional components, plumbing, and engineering efforts, which further contribute to the overall cost. Many automotive manufacturers are hesitant to transition to MHEs for EGR cooling owing to their higher costs. Nevertheless, there are experimental studies in which MHEs are used in waste-heat recovery applications to improve engine thermal efficiency [21,22].

This study aimed to assess the feasibility of using a high-efficiency compact MHE as an EGR cooler to meet the EURO 7 emission standards for heavy-duty diesel engines. A novel and noteworthy aspect of this study is the detailed explanation of the MHE sizing process, which sets it apart from previous studies. This study includes the development of detailed mathematical models for the mechanical and thermal-hydraulic design of the MHE. The performance of the MHE was rigorously evaluated, and its impact on the efficiency and emissions of heavy-duty diesel engines was assessed using Diesel-RK software. Calculations were conducted to determine the specific fuel consumption, NO_x emissions, and PM emissions for both the current engine setup and modified engine equipped with the proposed MHE cooler. By comparing the results, this study quantifies the potential improvements achieved through the implementation of the MHE cooler, providing valuable insights on emission reduction and engine optimization efforts.

2. System Description and Methods

An inline 6-cylinder diesel engine that is used as the prime mover for Ford F-Max 2023 model year heavy-duty trucks with 12.7 L engine displacement and Euro 6D-level emissions was selected from the literature [23] for this study. It has a power output of 500 PS (368 kW) at 1800 rpm and a torque of 2500 Nm between 1000 and 1200 rpm. The compression ratio is 17, and the cylinder bore is 130 mm with a stroke of 160 mm. The selected engine employs a high-pressure cooled EGR system, where the exhaust gas is taken downstream of the variable-geometry turbocharger (VGT) and fed back to the intake manifold after being cooled at the EGR cooler.

Throughout the course of this study, comprehensive mathematical models were developed to facilitate the mechanical and thermal-hydraulic design of the HX. Furthermore, the diesel engine being investigated was modeled using Diesel-RK software to assess its performance characteristics and calculate emissions. Figure 1 provides a visual representation of the design process adopted in this study. The first step involves the mechanical and thermal-hydraulic design of the MHE specific to EGR applications. This phase includes developing detailed mathematical models to optimize the MHE design that consider its mechanical aspects and thermal efficiency to achieve high performance. After the MHE is designed, the study progresses to the next stage, where the specifications of the newly designed MHE are integrated with the operational and hardware inputs of a heavy-duty diesel engine. Using these combined inputs, the specific fuel consumption (SFC) and emissions of the diesel engine are calculated using RK-Diesel software v4.3.0.189.

In Section 2.1 of this study, a comprehensive and detailed explanation of the diesel engine modeling process is presented. This includes the methodologies used and the various considerations taken into account during the modeling to accurately represent the behavior and performance of the diesel engine. Section 2.2 focuses on the mathematical model of the MHE used in this study. The key aspects of the mechanical and thermal-hydraulic models, including assumptions and equations, are thoroughly explained to provide a comprehensive understanding of their functionality.

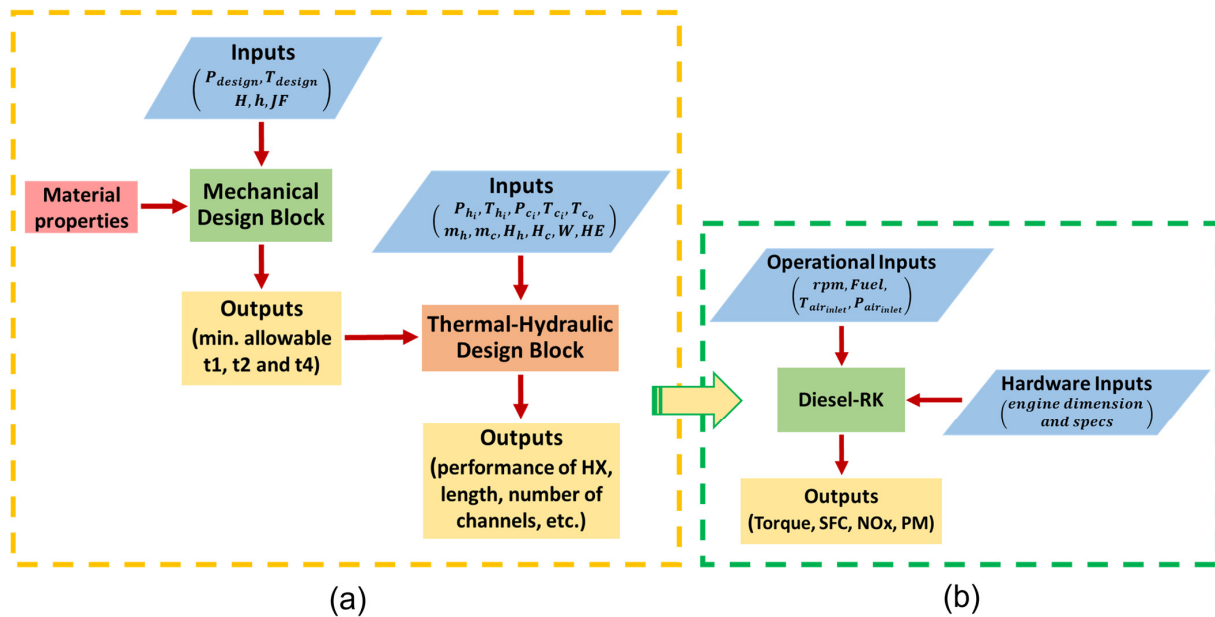


Figure 1. Schematic diagram for (a) HX design and (b) Diesel-RK calculations.

2.1. Diesel Engine Modeling in Diesel-RK

To estimate NO_x emissions, Diesel-RK software was used for the engine [24]. The modeling platform is a full-cycle thermodynamic engine development software program generated by Dr. Andrey Kuleshov, which allows users to model 2- and 4-stroke engines with emission prediction capability. Diesel-RK software has many capabilities, such as torque and power curves, engine performance, fuel consumption, and emissions analysis for both spark ignition and compression ignition combustion, and allows the user to employ advanced technologies, such as turbochargers and EGRs. The software was validated by considering a V8 heavy-duty diesel engine for medium (1400 rpm) and high (2100 rpm) operating engine speeds and 10%, 50%, and 100% loads for each operating speed. The fuel consumption prediction errors for each operating point with the order starting from the lowest engine speed and lowest load to the maximum engine speed and highest load are -2.4% , 4.9% , 3% , -3.8% , 0.9% , and 0% , respectively. Similarly, in the same order, the NO_x emission prediction errors were -7.1% , -11.5% , 1.4% , -20% , 13.7% , and 1.7% [25].

The analysis is performed at the rated power operating point with 500 PS and 1950 Nm torque at 1800 rpm engine speed, considering standard conditions of $25\text{ }^\circ\text{C}$ and 1 bar ambient temperature and pressure, respectively. Air and fuel properties such as flow rate, temperature, and pressure values for the rated power operating point are listed in Table 1. The compressor and turbine parameters, such as efficiency and fuel injection values, are determined by tuning the engine output torque at the rated power operating point. The EGR cooler inlet temperature was set to $550\text{ }^\circ\text{C}$ based on a previous study [10]. Geometric dimensions for the piston bowl design are shown in Figure 2, and values used during this study are listed in Table 2.

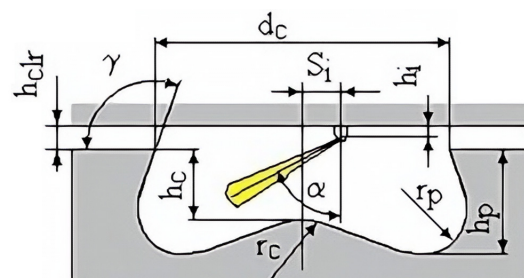


Figure 2. Piston bowl geometry and design parameters.

Table 1. Simulation point turbocharger boundary conditions and EGR operating parameters.

Parameter	Value
Total pressure after induction air filter (mbar)	980
Exhaust back pressure (after turbine—absolute) (mbar)	1180
Exhaust gas recirculation ratio	0.1484
Average total turbine inlet temperature (°C)	550
Intercooler outlet temperature (°C)	45
Total air fuel ratio (Lambda)	1.5126
Total mass intake airflow of the engine (kg/s)	0.4592
Mass of fuel supplied per cycle (g)	0.2327

Table 2. Piston bowl geometric design parameters.

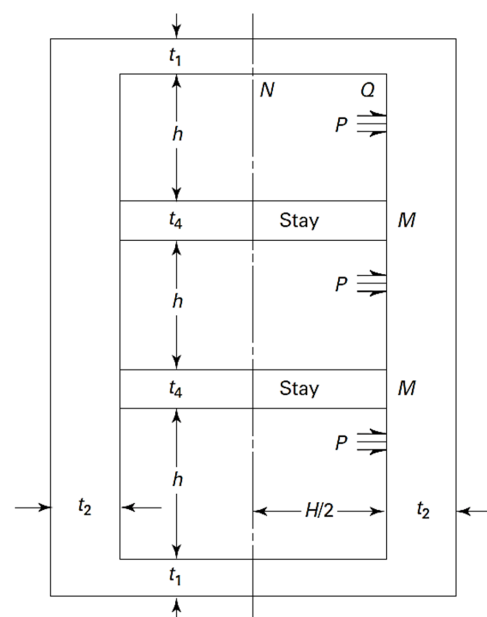
Parameter	Value
External diameter, d_c (mm)	84.3
In-center piston bowl depth, h_c (mm)	7.52
Radius of sphere in the center of the piston bowl, r_c (mm)	22.3
Depth of the combustion chamber in periphery, h_p (mm)	23.4
Radius of hollow chamber in periphery of the bowl, r_p (mm)	10.2
Inclination angle of the bowl forming to the plane of the piston crown, γ (deg)	90
Clearance at TDC, h_{clr} (mm)	2

2.2. Microchannel Heat Exchanger Design

During the design of the microchannel heat exchanger (MHE), various criteria, such as compactness, thermal load, maximum pressure, maximum temperature, and suitable plate thickness for manufacturing, should be considered. In this section, the MHE design is explained under the subsections of mechanical design and thermal-hydraulic design.

2.2.1. Mechanical Design

The mechanical design of the MHE has been made in accordance with ASME BPVC (Rules for the Fabrication of Pressure Vessels) VIII Part 1, UG-19 Special Constructions Section and Mandatory Annex 13-9. The E (joint factor) value used in the equations is given as 0.7 for diffusion bonding and 0.5 for brazing [26]. The dimensions of the rectangular cross-section of the pressure vessel used in the design are shown in Figure 3.

**Figure 3.** Rectangular cross-section supported by stayed plates [26].

During the mechanical design calculations, the stayed plate thickness t_4 , thin wall thickness t_2 , and side margin thickness t_1 were identified as the three critical thicknesses of interest in the stress analysis of rectangular pressure vessels. The minimum values of t_1 , t_2 , and t_4 were determined based on the following criteria:

1. The membrane stress in the stayed plate S_m^{stay} , in the long side of vessel S_m^L , and in the short side of vessel S_m^S shall not exceed the design stress, i.e., $S_m^{stay} \leq S E$, $S_m^L \leq S E$ and $S_m^S \leq S E$, where S and E are the maximum allowable stress and joint factor, respectively.
2. The total stress in the stay plate S_t^{stay} , which is equal to S_m^{stay} , shall not exceed 1.5 times the design stress, i.e., $S_t^{stay} = S_m^{stay} \leq 1.5 S$.
3. The total stress in the long side S_t^L , which is the sum of the membrane S_m^L and bending stress S_b^L , shall not exceed 1.5 times the design stress, i.e., $S_t^L = S_m^L + S_b^L \leq 1.5 S E$.
4. The total stress at location N (Figure 3) S_t^N , which is the sum of the membrane S_m^S and bending stress S_b^N at location N , shall not exceed 1.5 times the design stress, i.e., $S_t^N = S_m^S + S_b^N \leq 1.5 S E$.
5. The total stress at location Q in the short side S_t^{QS} , which is the sum of the membrane S_m^S and bending stress S_b^{QS} at location Q , shall not exceed 1.5 times the design stress, i.e., $S_t^{QS} = S_m^S + S_b^{QS} \leq 1.5 S E$.
6. The total stress at location Q in the long side S_t^{QL} , which is the sum of the membrane S_m^S and bending stress S_b^{QL} at location Q , shall not exceed 1.5 times the design stress, i.e., $S_t^{QL} = S_m^S + S_b^{QL} \leq 1.5 S E$.

The stress values were computed using the following equations:

$$S_m^{stay} = \frac{Ph}{2t_4} \left\{ \frac{6 + K(11 - \alpha^2)}{3 + 5K} \right\} \quad (1)$$

$$S_m^L = \frac{PH}{2t_2} \quad (2)$$

$$S_m^S = \frac{Ph}{2t_1} \left\{ 3 - \left[\frac{6 + K(11 - \alpha^2)}{3 + 5K} \right] \right\} \quad (3)$$

$$S_b^L = \frac{Ph^2 c_2}{12I_2} \left[\frac{3 + K(6 - \alpha^2)}{3 + 5K} \right] \quad (4)$$

$$S_b^N = \frac{Pc_1}{24I_1} \left[-3H^2 + 2h^2 \left(\frac{3 + 5\alpha^2 K}{3 + 5K} \right) \right] \quad (5)$$

$$S_b^{QS} = \frac{Ph^2 c_1}{12I_1} \left(\frac{3 + 5\alpha^2 K}{3 + 5K} \right) \quad (6)$$

$$S_b^{QL} = \frac{Ph^2 c_2}{12I_2} \left(\frac{3 + 5\alpha^2 K}{3 + 5K} \right) \quad (7)$$

where P is the design pressure, and K , α , c_1 , c_2 , I_1 , and I_2 can be calculated using

$$K = \frac{I_2}{I_1} \alpha, \quad \alpha = \frac{H}{h}, \quad c_1 = \frac{t_1}{2}, \quad c_2 = \frac{t_2}{2}, \quad I_1 = \frac{t_1^3}{12} \quad \text{and} \quad I_2 = \frac{t_2^3}{12}. \quad (8)$$

The variation in the maximum allowable stress with temperature for the SS316–316 L dual-grade material used in the design is shown in Figure 4.

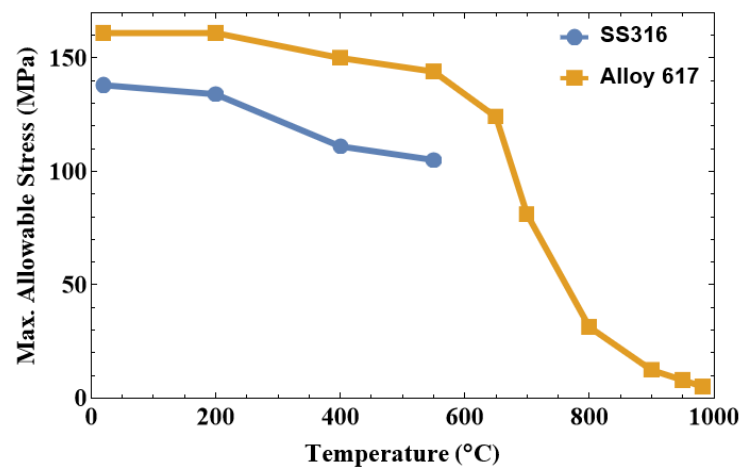


Figure 4. The maximum allowable stress with temperature for the SS316–316 L dual-grade and alloy 617.

In the mechanical design of the MHE, certain parameters were predetermined, including the channel height, width, design pressure, and temperature. Based on these initial values, minimum thickness values were calculated, and final values were selected considering cost and ease of manufacturing. The coupling factor for the brazing application was chosen as $E = 0.5$. The design pressure was set at 3.75 bar, and the design temperature was 550 °C. Table 3 presents the dimensions obtained under these conditions, which include the selected thickness values. These thickness values are crucial in subsequent thermal-hydraulic design calculations, which will be detailed in the following subsection of this study.

Table 3. EGR cooler thickness parameters.

Parameter	Value
Thin wall thickness (t_2) (mm)	0.5
Stayed plate thickness (t_4) (mm)	0.5
Side margin thickness (t_1) (mm)	3.75

2.2.2. Thermal-Hydraulic Design

The sub-heat exchanger model shown in Figure 5 is used in the thermal-hydraulic design process. In this model, the HX is divided into sub-heat exchanger parts, and performance analyses are carried out for each part. Total heat load of the MHE is equally distributed to each sub-HX. The lengths of the sub-heat exchangers are calculated based on the analysis, and the total length of the HX is obtained by summing the length of each sub-heat exchanger [27]. The fin efficiency is also taken into consideration to enhance the accuracy of calculations in the mathematical model applied during the critical design phase.

The calculations begin by determining the number of hot and cold channels from the given overall width (W) and height (HE) of the HX using the following equations:

$$N_{ch} = \frac{HE - t_2}{2t_2 + H_h + H_c} \quad (9)$$

$$N_{fin} = \frac{W - (h + 2t_4)}{h + t_4} \quad (10)$$

where N_{ch} is the number of hot or cold channels, N_{fin} is the number of fins, h is the width of the channel, and H_h and H_c are the hot and cold channel depths, respectively (Figure 6).

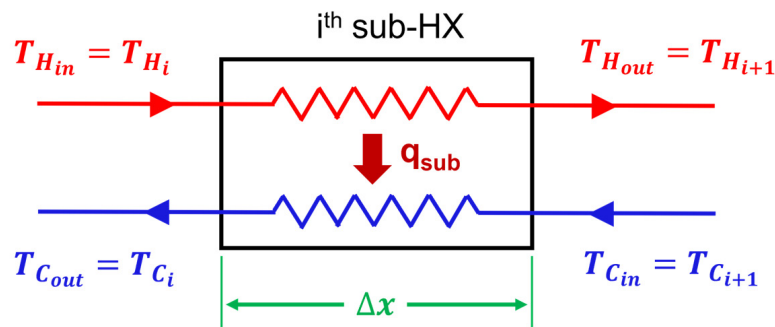
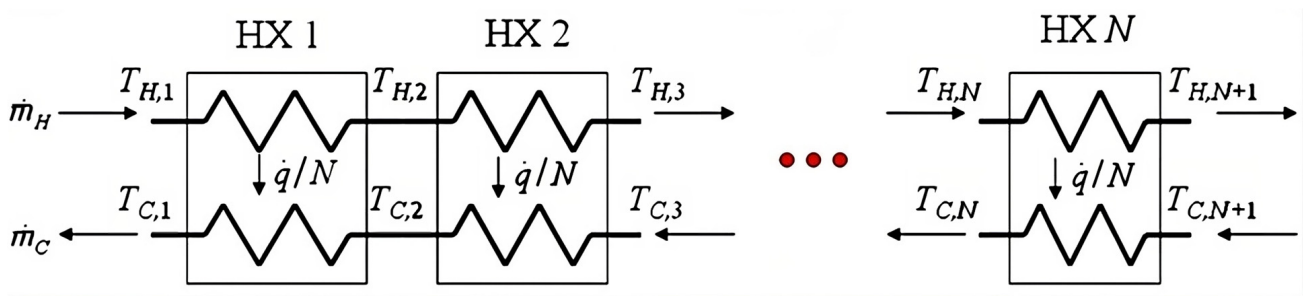


Figure 5. Sub-heat exchanger model. Modified from [27].

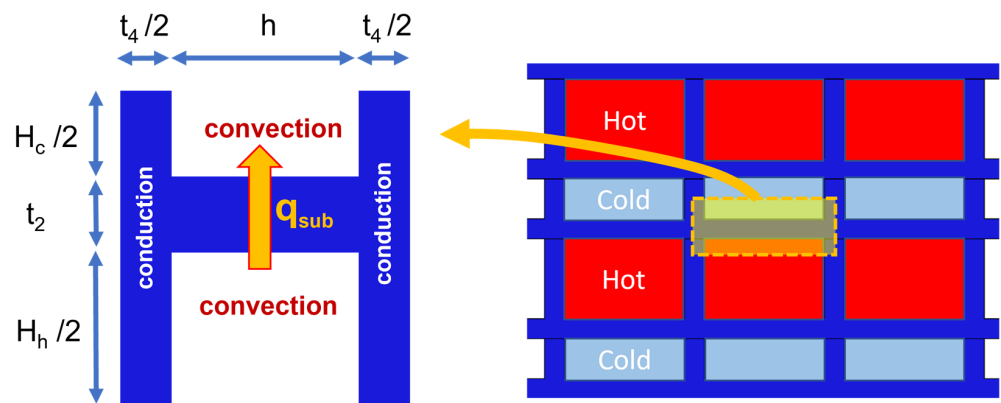


Figure 6. Channel geometry.

Compactness (β) of an HX refers to the ratio of the heat-transfer surface area to the corresponding HX core volume. It has a unit of m^2/m^3 and can be determined by the following equation:

$$\beta = \frac{2h + H_h + H_c}{(h + t_4) \left(\frac{H_h + H_c}{2} + t_2 \right)} \tag{11}$$

Once the number of channels is determined, the next step is to determine the total heat load of the HX (Q) and unknown hot fluid outlet temperature ($T_{h_{out}}$) by using this equation:

$$\dot{Q} = \dot{m}_c C_{P_c} (T_{c_{out}} - T_{c_{in}}) = \dot{m}_h C_{P_h} (T_{h_{out}} - T_{h_{in}}) \tag{12}$$

where \dot{m}_h , \dot{m}_c , $T_{h_{in}}$, $T_{c_{in}}$, and $T_{c_{out}}$ are hot fluid mass flow rate, cold fluid mass flow rate, hot fluid inlet temperature, cold fluid inlet temperature, and cold fluid outlet temperature, respectively.

If the number of sub-heat exchangers for the analysis is N , then the heat transfer in each sub-heat exchanger is

$$\dot{q}_{sub} = \frac{\dot{Q}}{N} \tag{13}$$

The HX has a counterflow arrangement, and for each sub-heat exchanger inlet temperature of the hot and cold fluids, the mass flow and heat-transfer rates are known. Therefore, the effectiveness (ϵ), NTU , and UA of the i -th sub-exchanger can be computed using the following equations [28]:

$$\epsilon_i = \frac{\dot{q}_{sub}}{C_{min}^i (T_{hin}^i - T_{cin}^i)} \quad (14)$$

$$NTU_i = \frac{1}{CR_i - 1} \ln \left[\frac{\epsilon_i - 1}{\epsilon_i CR_i - 1} \right] \quad (15)$$

$$U_i A_i = NTU_i C_{min}^i \quad (16)$$

where the heat capacity rate ratio (CR) is equal to C_c/C_h or C_h/C_c , depending on the relative magnitudes of the hot and cold fluid heat capacity rates, respectively. U_i is the overall heat-transfer coefficient, A_i is the heat-transfer surface area, and C_{min}^i is the minimum of C_c and C_h for the i -th sub-exchanger.

$U_i A_i$ for the sub-heat exchanger can also be found from the thermal resistance network shown in Figure 7 by using the equation

$$U_i A_i = \frac{1}{R_{tot_i}} \quad (17)$$

where R_{tot_i} is the total resistance of the network and can be calculated by

$$R_{tot_i} = \frac{1}{\frac{1}{R_{fin,c_i}} + \frac{1}{R_{conv,c_i}}} + R_{cond_i} + \frac{1}{\frac{1}{R_{fin,h_i}} + \frac{1}{R_{conv,h_i}}} \quad (18)$$

where R_{fin} , R_{cond} , and R_{conv} are the conduction resistance of fin, conduction resistance of wall, and convection resistance, respectively.

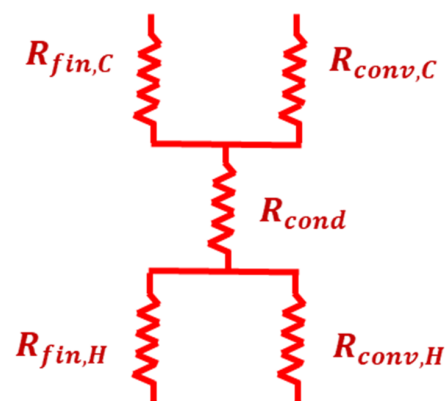


Figure 7. Thermal resistance network.

The thermal resistance terms are computed using the following equations:

$$R_{conv_i} = \frac{1}{h_{conv_i} (\Delta x_i)} \quad (19)$$

$$R_{cond_i} = \frac{t_2}{k_{wall} ((h + t_4) \Delta x_i)} \quad (20)$$

$$R_{fin_i} = \frac{1}{\eta_f h_{conv_i} ((\Delta x_i + t_4) H)} \quad (21)$$

where Δx_i is the length of the i -th sub-heat exchanger, k_{wall} is the thermal conductivity of the HX material, h_{conv} is the convection heat-transfer coefficient, and η_f is the fin efficiency.

R_{conv} and R_{fin} are different on hot and cold fluid sides because of different h_{conv} and H values on each side.

Assuming an adiabatic fin tip, the fin efficiency can be found as follows [28]:

$$\eta_{fi} = \frac{\text{Tanh}[m_i L_c]}{m_i L_c} \quad (22)$$

where the corrected length (L_c) and m are given by (assuming $\Delta x \gg t_4$):

$$L_c = \frac{H + t_4}{2} \text{ and } m_i = \sqrt{\frac{2h_{conv i}}{k_{wall} t_4}} \quad (23)$$

The convection heat-transfer coefficient is determined using the nondimensional Nusselt number (Nu) as follows:

$$h_{conv i} = \frac{Nu_i k_{fluid}}{D_h} \quad (24)$$

where k_{fluid} is the thermal conductivity of the fluid flowing through the channels, and D_h is the hydraulic diameter, which can be expressed as

$$D_h = \frac{2hH}{h + H} \quad (25)$$

The pressure drop across the i -th sub-heat exchanger core (ΔP_i) is given by the Darcy–Weisbach equation:

$$\Delta P_i = f_i \frac{\rho_i u_i^2}{2} \frac{\Delta x_i}{D_h} \quad (26)$$

where f is the Darcy friction factor, u is the fluid velocity, and ρ is the fluid density.

Nusselt number (Nu) and Darcy friction factor (f) correlations depend on the flow type. If the Reynolds number (Re) is less than 2300, the flow is assumed to be laminar, and if it is greater than 2300, it is assumed to be turbulent.

For a fully developed laminar flow through rectangular ducts, the Darcy friction factor equation is expressed as follows [29]:

$$f_{lam} = \frac{96}{Re} \left(1 - 1.3553\alpha + 1.9467\alpha^2 - 1.7012\alpha^3 + 0.9564\alpha^4 - 0.2537\alpha^5 \right) \quad (27)$$

where α is the channel aspect ratio defined as $\alpha = \frac{\text{short side length}}{\text{long side length}}$.

The Nusselt number correlation for a fully developed laminar flow through rectangular ducts with constant axial wall heat flux and constant peripheral wall temperature is expressed as follows [29]:

$$Nu_{lam} = 8.235 \left(1 - 2.0421\alpha + 3.0853\alpha^2 - 2.4765\alpha^3 + 1.0578\alpha^4 - 0.1861\alpha^5 \right) \quad (28)$$

For turbulent flow, the Nusselt correlation valid for smooth tubes over a large Reynolds number range, including the transition region, is provided by Gnielinski as follows [30]:

$$Nu_{turb} = \frac{(f/8)(Re - 1000)Pr}{1 + 12.7(f/8)^{0.5}(Pr^{2/3} - 1)} \quad (29)$$

where the Darcy friction factor can be obtained from an approximate explicit relation given by the following [31]:

$$\frac{1}{\sqrt{f_{turb}}} = -2 \log_{10} \left[\frac{e/D_h}{3.7} - \frac{5.02}{Re_D} \log_{10} \left[\frac{e/D_h}{3.7} + \frac{13}{Re_D} \right] \right] \quad (30)$$

The aim of the design is to calculate the HX length, pressure, and temperature variations along the HX. The main steps of the thermal-hydraulic calculation are summarized in Figure 8. For the given input values, the code calculates the outlet temperature, pressure drop, and length of each sub-HX and, finally, combines these results to obtain the overall values for the MHE.

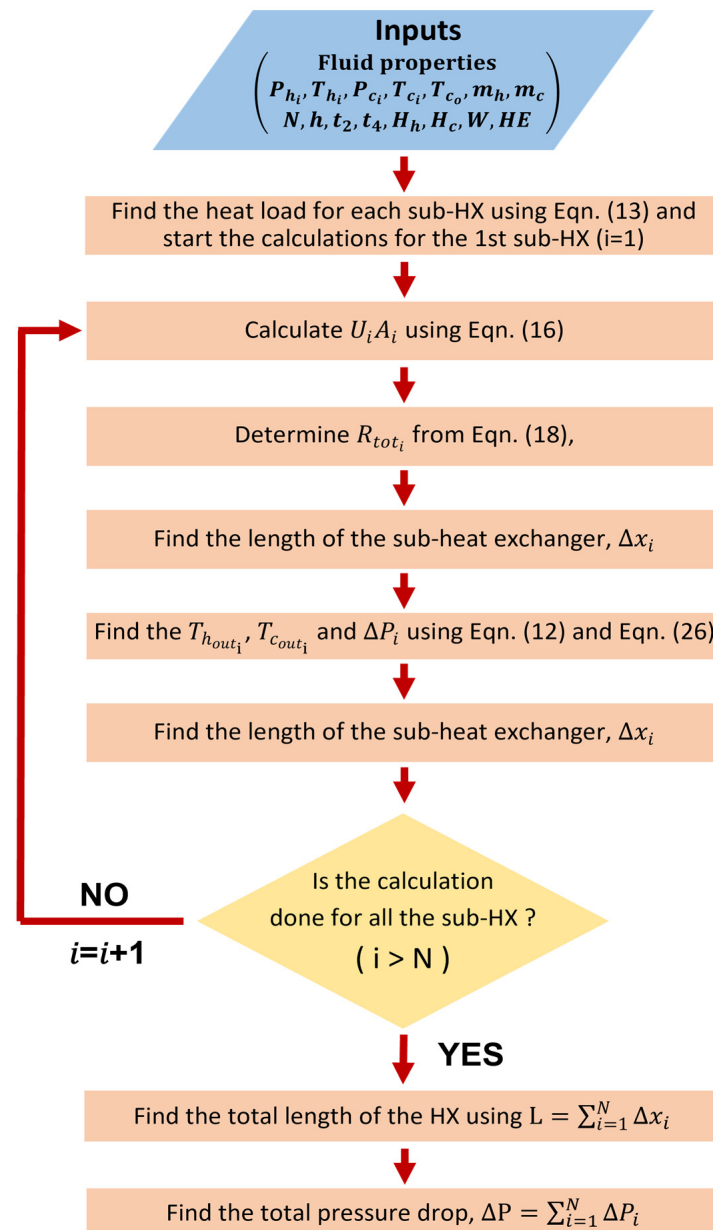


Figure 8. Flowchart for the HX thermal-hydraulic calculations.

3. Results and Discussion

The results of this study are summarized in the following two subsections. The first subsection presents the optimization and performance analysis of the MHE, and the second subsection focuses on engine performance and emissions.

3.1. Microchannel Heat Exchanger Design Results

Table 4 summarizes the boundary conditions and constraints of the EGR cooler. These values are either calculated or determined based on the specifications of the 500 PS diesel engine under consideration. Throughout the calculations, these parameters are fixed, and

the overall HX height (HE), width (W), channel depth (H), and channel width (h) are varied to obtain the optimum thermal-hydraulic performance for the minimum HX dimensions.

Table 4. Inputs for the EGR cooler design.

Parameter	Value	Parameter	Value
T_{hin} (°C)	550	T_{cin} (°C)	50
P_{hin} (bar)	2.3	T_{cout} (°C)	59
\dot{m}_h (kg/s)	0.08	P_{cin} (bar)	2.0
t_2 (mm)	0.5	\dot{m}_c (kg/s)	1.0
t_4 (mm)	0.5	N	10
ΔP_{cmax} (mbar)	100	ΔP_{hmax} (mbar)	30

Changing the overall height and width of the HX while keeping the channel dimensions fixed affects the number of hot and cold channels. For a fixed mass flow rate, the channel number changes the fluid velocity through each channel, which changes the convection heat-transfer coefficient, thereby resulting in HX length variation. This effect can be observed in Figure 9, which shows the impact of height and width on the total length of the HX. Increasing the height or the width while keeping the other fixed first increases the length and then decreases it. This can be explained as follows: Initially, increasing the number of channels decreases the fluid velocity, which decreases the convection heat-transfer coefficient. Therefore, a larger channel length (i.e., a larger heat-transfer surface area) is required to satisfy the heat-transfer rate requirement. Subsequently, the increase in the number of channels outperforms the decrease in the heat-transfer coefficient, and the channel length starts to decrease.

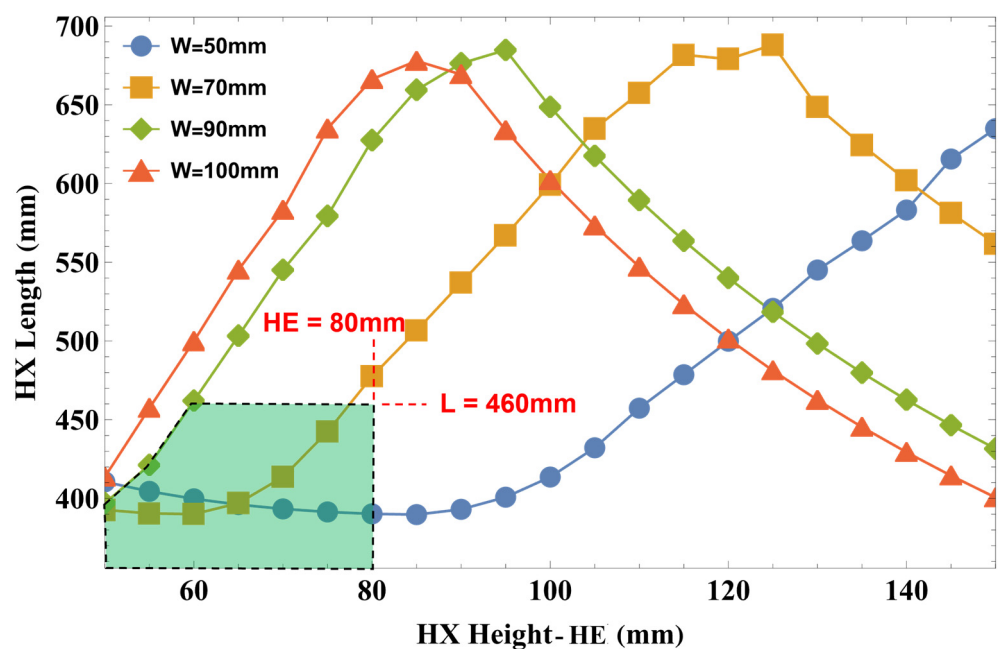


Figure 9. HX length variation with respect to overall height and width.

The EGR cooler core dimensions currently used in the 500 PS diesel engine under investigation are listed in Table 5. In this study, one of the objectives is to design a more compact EGR cooler. Therefore, the dimensions of the new EGR should be smaller than those of the current one, and the green shaded region in Figure 9 provides a suitable domain for the dimensions of the new design. To select the overall height and width, the variations in HX core mass and pressure losses with respect to these parameters must be considered. As demonstrated in Figure 10c,d, increasing the height or width decreases the pressure losses; however, it increases the mass. Hence, choosing the dimensions of the heat

exchanger involves finding a balance between minimizing the pressure loss and managing the mass and size of the heat exchanger. Increasing the channel dimensions can reduce the pressure drop. However, this comes at the cost of a larger and heavier heat exchanger owing to the additional material required.

Table 5. Current EGR core dimensions.

Parameter	Value
Height (HE) (mm)	80
Width (W) (mm)	90
Length (L) (mm)	460

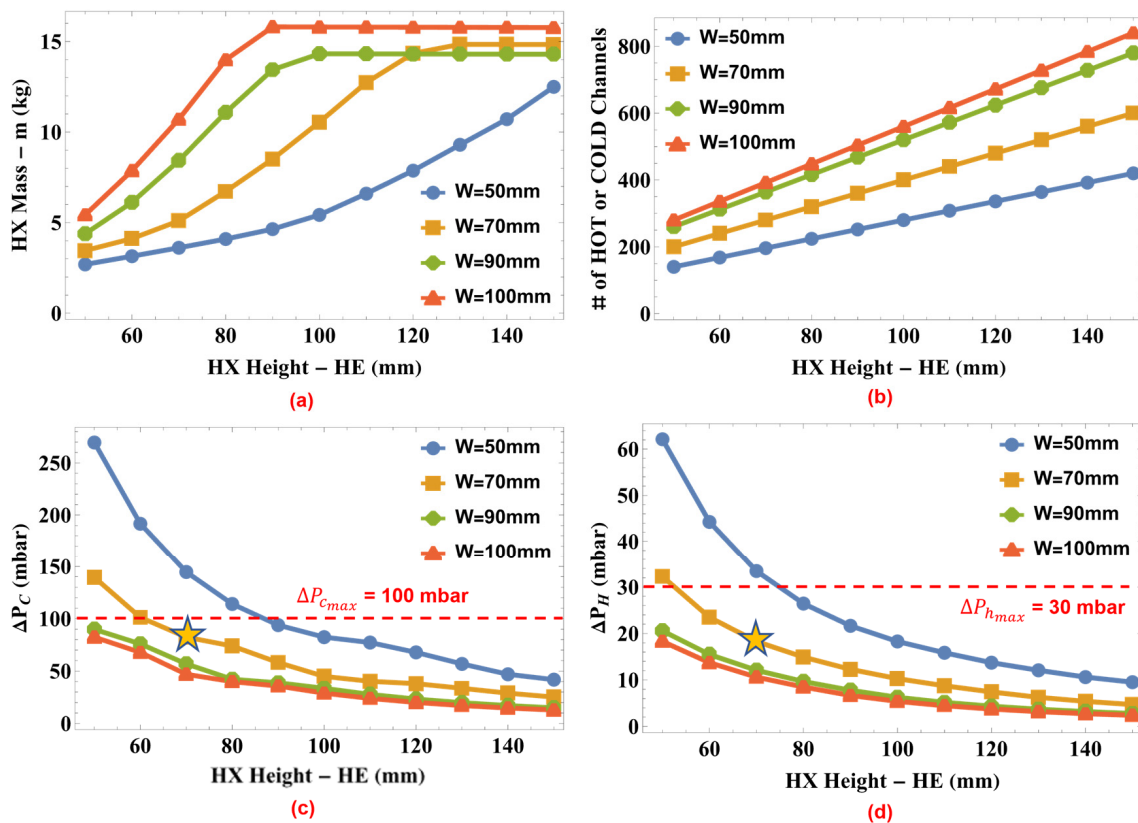


Figure 10. Change in (a) heat exchanger core mass, (b) number of channels, (c) cold fluid pressure loss, and (d) hot fluid pressure loss with respect to overall height and width.

Considering the target pressure losses of 100 mbar and 30 mbar on the cold and hot fluid sides, respectively, both the overall height and width were selected to be 70 mm; the design points can be seen in Figure 10c,d (stars on the figures). These dimensions were used during the optimization of channel depth and width.

Figure 11 shows the effect of channel width (h) and depth (H) on the HX length. As illustrated in the figure, increasing the width or depth increases the length of the HX. However, the effect of channel depth is more dominant than the effect of channel width. This can be realized by considering two points in Figure 10: point 1 where $h = 2$ mm and $H = 3$ mm, and point 2 where $h = 3$ mm and $H = 2$ mm. Although the two points have the same cross-sectional flow area, point 2, which has a smaller depth and higher width, results in a smaller HX length. This is because a smaller depth implies shorter fins, which results in higher-efficiency fins. As the fin efficiency increases, the conduction resistance through the fin decreases, which increases the overall heat-transfer coefficient (U) and consequently decreases the heat-transfer surface area requirement and length of the HX.

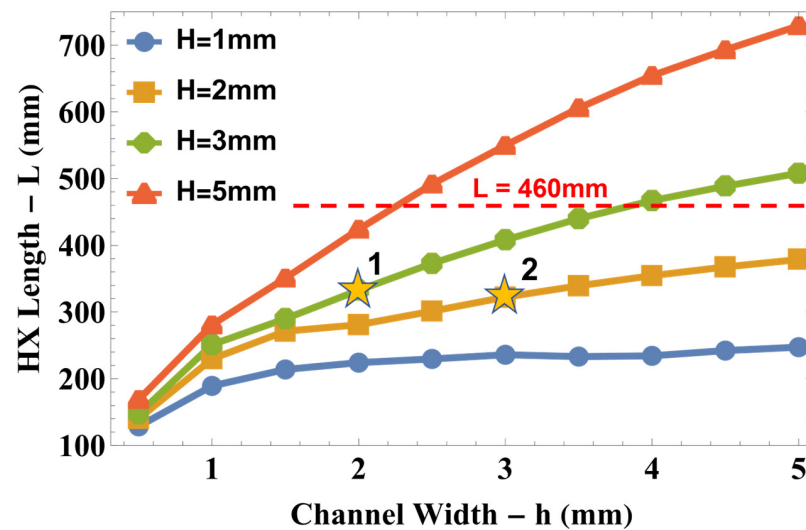


Figure 11. Effect of channel dimensions on overall HX length.

Figure 12 shows the pressure drop on the cold fluid side (a) and hot fluid side (b) with the channel width and depth. As depicted in the figure, the trend of decreasing pressure loss with increasing width and depth of the channels aligns with the expectations. This result is in line with the principle that the pressure loss is directly proportional to the square of fluid velocity. When the channel dimensions are increased, the cross-sectional area of the flow also increases. For a fixed mass flow rate, this expansion in the cross-sectional area leads to a reduction in fluid velocity. Consequently, the pressure loss decreases accordingly.

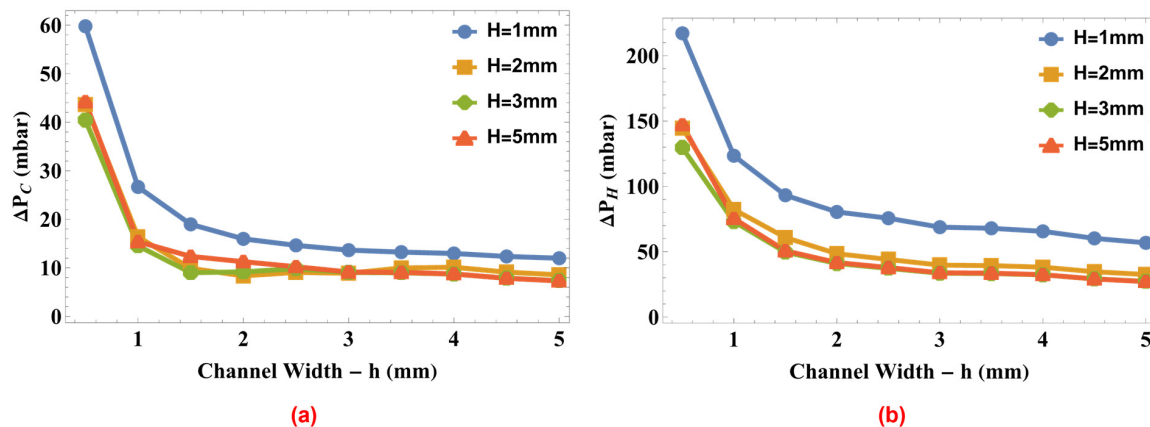


Figure 12. Effect of channel dimensions on (a) cold fluid and (b) hot fluid pressure loss.

The optimum channel dimensions for the hot and cold fluid sides were determined based on the target of having the highest thermal-hydraulic performance for the minimum HX dimensions. Table 6 shows the core dimensions of the EGR cooler after the mechanical and thermal-hydraulic optimization studies. Table 7 lists the thermal-hydraulic performance of the new EGR cooler. It has an effectiveness of 0.89 and is capable of rejecting 37.6 kW heat although it has much smaller dimensions than the current cooler.

Once the dimensions of the MHE are determined for the required boundary conditions, thermal-hydraulic performance of the design is investigated. Figure 13 shows the changes in the temperature (a) and pressure (b) of the hot and cold fluids along the flow direction. Arrows on the figures show the direction of the flow. The pressure drop on the cold fluid side (i.e., the coolant, water, in this case) is 82 mbar, while the pressure drop on the hot fluid side (exhaust gases) is 18 mbar. The temperature change on the hot fluid side was greater than that on the cold fluid side because the heat capacity rate on the hot fluid side

was smaller. The exit temperatures of the hot exhaust gas and cooling water are 103.5 °C and 59 °C, respectively. The EGR cooler was designed to operate at exhaust temperatures above 100 °C, because temperatures below this value result in the condensation of sulfuric acid in the EGR cooler, causing the cooler to corrode and foul. The potential for EGR cooler outlet temperatures to decrease below 100 °C at other operating points and conditions is an existing challenge, not limited to the proposed MHE design. This issue is relevant for current EGR cooler types as well. However, the proposed design, which includes a second cooling circuit, offers a notable advantage in addressing this challenge. With the addition of a second cooling circuit, controlling the EGR cooler outlet temperature becomes significantly more manageable.

Table 6. Heat exchanger core specifications.

Parameter	Value
Channel width (h) (mm)	3
Channel depth (hot side— H_h) (mm)	3
Channel depth (cold side— H_c) (mm)	1
Thin wall thickness (t_2) (mm)	0.5
Stayed plate thickness (t_4) (mm)	0.5
Side margin thickness (t_1) (mm)	3.75
Length (L) (mm)	414
Width (W) (mm)	70
Height (HE) (mm)	70
Core mass (kg)	5.1
No. of plates (hot + cold)	14 + 14 = 28
No. of channels on a single plate	20
Compactness (β) (m^2/m^3)	1143

Table 7. Thermal-hydraulic performance results.

Parameter	Value
Q (kW)	37.6
ΔP_c (mbar)	82
ΔP_h (mbar)	18
$T_{h_{out}}$ (°C)	103.5
LMTD (°C)	197.3
U_c ($W/m^2.K$)	205.9
U_h ($W/m^2.K$)	137.3
NTU	2.26
E	0.89

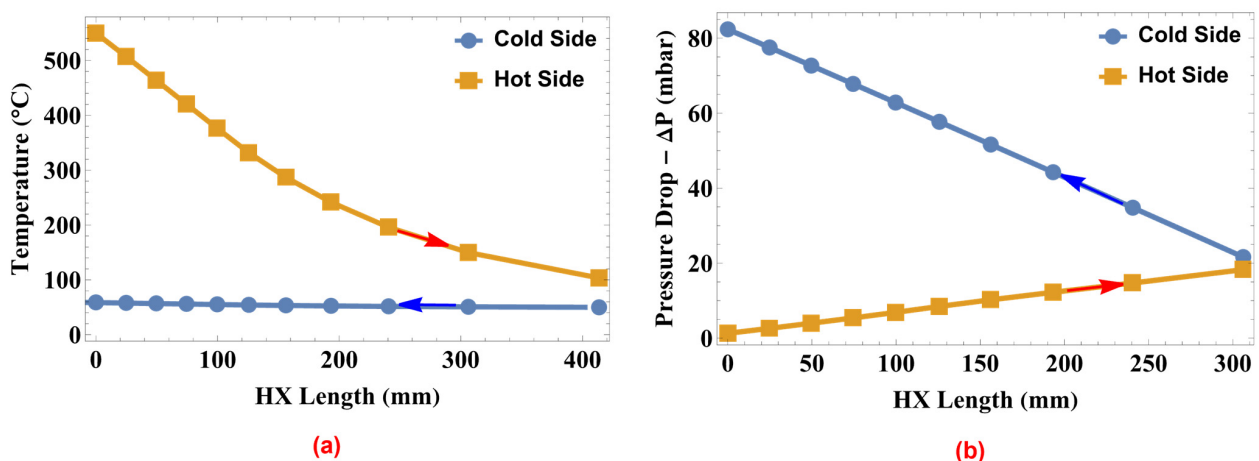


Figure 13. Temperature (a) and pressure (b) variations along the flow direction.

Figure 14 shows the 3D model of the designed EGR cooler. It has 14 cold plates and 14 hot plates. Each plate had 20 channels; therefore, the final design consists of 280 hot and 280 cold channels and has a compactness value of $1143 \text{ m}^2/\text{m}^3$.

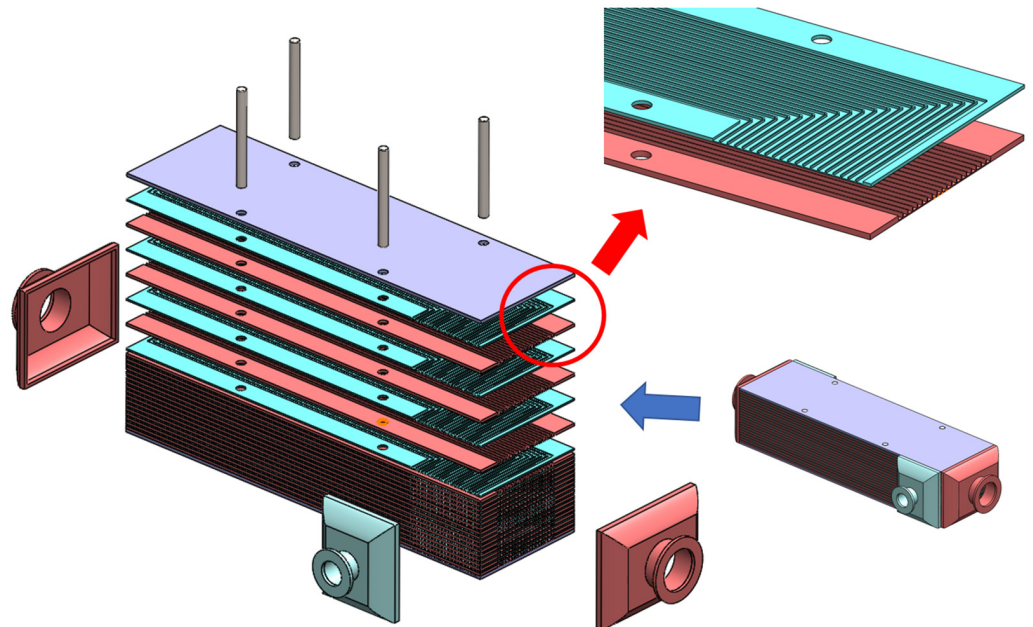


Figure 14. New EGR cooler 3D model.

3.2. Diesel-RK Engine Performance Simulation Results

In the original heavy-duty diesel engine configuration, the cooling effectiveness of the EGR cooler is 0.7, with an exhaust gas flow rate of 0.08 kg/s. Using Diesel-RK software, the simulation for this configuration resulted in an outlet temperature of $182.7 \text{ }^\circ\text{C}$ for the exhaust gases, given their $550 \text{ }^\circ\text{C}$ inlet temperature. The specific fuel consumption (SFC) is calculated to be 205.51 g/kWh , while NO_x emissions and PM emissions are determined to be 3.6194 g/kWh and 0.1422 g/kWh , respectively.

To study the impact of the EGR cooler effectiveness on engine performance and emissions, a parametric simulation is conducted by increasing the EGR cooler effectiveness from 0.7 to 0.85, with increments of 0.025. This study analyzed two cases: one with a constant EGR ratio, leading to an increased EGR mass, and the other with a constant EGR mass, resulting in a reduced EGR ratio. The results of these simulations are presented in Tables 8 and 9, respectively.

Table 8. Fuel economy and emission results for constant EGR ratio values.

Power	EGR Mass	Cooler Eff.	EGR In Temp.	EGR Out Temp.	SFC	NO_x	PM
(kW)	(kg/s)	(%)	($^\circ\text{C}$)	($^\circ\text{C}$)	(g/kWh)	(g/kWh)	(g/kWh)
366.9	0.08002	0.700	551	182.7	205.51	3.6194	0.1422
368.6	0.08056	0.725	546	168.3	205.05	3.5464	0.1384
368.6	0.08099	0.750	543	154.4	205.04	3.5218	0.1348
367.4	0.08140	0.775	534	139.5	204.66	3.4770	0.1316
367.2	0.08170	0.800	534	126.8	204.63	3.4814	0.1304
368.6	0.08210	0.825	528	113.0	204.20	3.3829	0.1286
367.9	0.08243	0.850	526	100.1	204.21	3.3631	0.1260

Additionally, to better understand the relationship between the EGR cooler outlet temperatures and variations in SFC, NO_x emissions, and PM emissions, linear trend lines are fitted to the data extracted from Tables 8 and 9. The resulting trends are visually repre-

sented in Figure 15, Figure 16, and Figure 17 for SFC, NO_x, and PM emissions, respectively.

Table 9. Fuel economy and emission results for constant EGR mass values.

Power	EGR Mass	Cooler Eff.	EGR In Temp.	EGR Out Temp.	SFC	NO _x	PM
(kW)	(kg/s)	(%)	(°C)	(°C)	(g/kWh)	(g/kWh)	(g/kWh)
366.9	0.08002	0.700	551	182.7	205.51	3.6194	0.1422
367.7	0.08002	0.725	549	169.0	205.21	3.6547	0.1372
368.1	0.08000	0.75	540	153.8	205.03	3.5981	0.1336
367.4	0.08001	0.775	537	140.0	204.75	3.5773	0.1316
368.3	0.08001	0.800	534	126.7	204.51	3.5524	0.1300
368.4	0.08000	0.825	528	113.0	204.29	3.5063	0.1278
368.3	0.08002	0.850	526	100.1	204.08	3.5009	0.1257

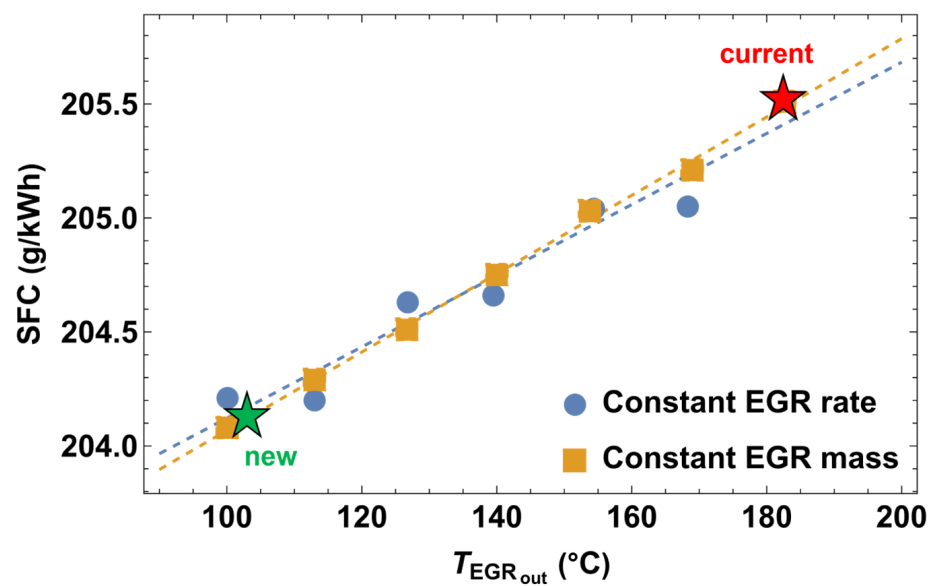


Figure 15. Simulated SFC variation with respect to EGR cooler outlet temperature.

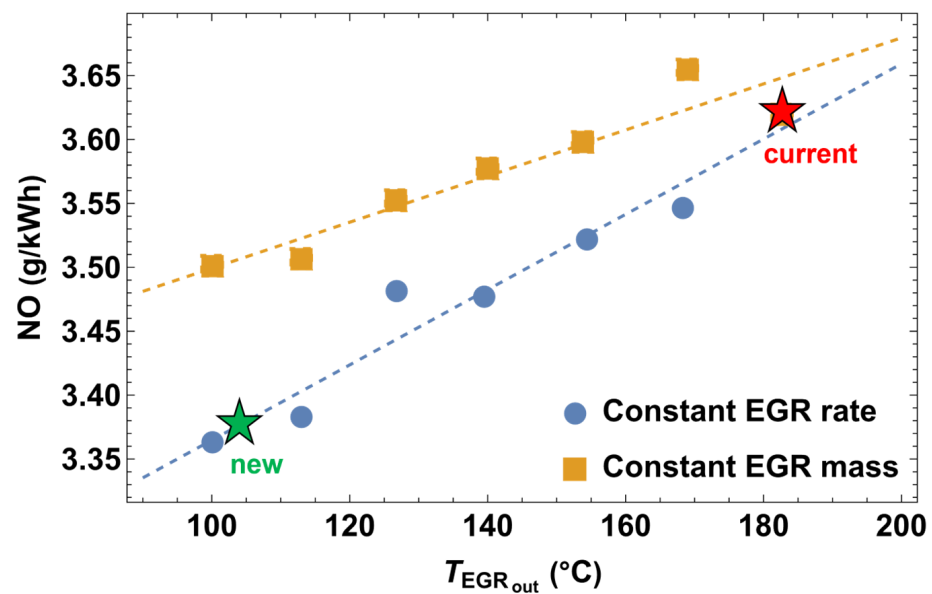


Figure 16. Simulated NO_x emissions variation with respect to EGR cooler outlet temperature.

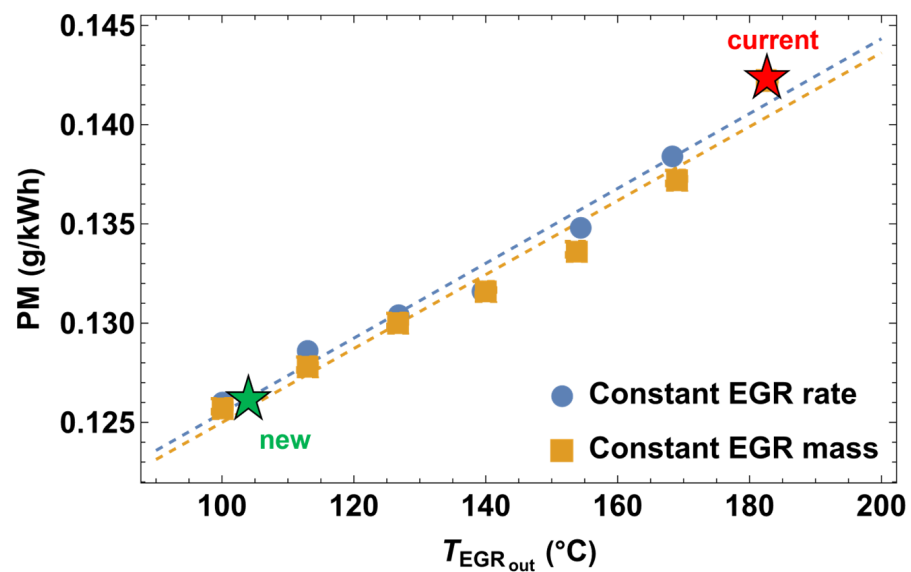


Figure 17. Simulated PM emissions variation with respect to EGR cooler outlet temperature.

Considering the constant EGR ratio case, increasing the EGR cooler effectiveness results in a reduced EGR cooler outlet temperature that mixes with the clean boost air and forms a cooler intake mixture temperature. This situation improves the volumetric efficiency of the diesel engine, and as a result, both the clean air and EGR mass values increase, reducing the engine outlet (EGR inlet) temperature. The SFC value improves by approximately 1.33 g/kWh (0.65%) for an EGR cooler outlet temperature reduction of 82.6 °C. Under these conditions, the NO_x and PM emissions improve by 0.2443 g/kWh (6.75%) and 0.0161 g/kWh (11.30%), respectively. For the constant EGR mass case, the SFC value improves around 1.38 g/kWh (0.67%) for an EGR cooler outlet temperature reduction of 82.6 °C. Under these conditions, NO_x and PM emissions improve to 0.1139 g/kWh (3.15%) and 0.0166 g/kWh (11.64%), respectively. A comprehensive analysis between these two cases clearly shows that improving the EGR cooler effectiveness allows a higher EGR mass in the combustion chamber while maintaining the current EGR ratio and significantly reduces NO_x emissions without compromising the fuel economy and PM emissions values similar to the literature correlations. As the EGR ratio was constant, the effect on combustion stability was almost negligible. Considering the constant EGR mass case, the reduction in NO_x emissions is limited to 3.15% because of the incomplete use of the EGR capability of the engine.

The proposed microchannel EGR cooler is capable of reducing the exhaust gas outlet temperature to 103.5 °C. Therefore, SFC, NO_x, and PM are evaluated at this outlet temperature and the results are tabulated in Table 10 for both the current and newly proposed EGR coolers.

Table 10. Fuel economy and emission prediction for the proposed EGR cooler.

	Constant EGR Rate			Constant EGR Mass		
	SFC	NO _x	PM	SFC	NO _x	PM
	(g/kWh)	(g/kWh)	(g/kWh)	(g/kWh)	(g/kWh)	(g/kWh)
Current EGR	205.51	3.6194	0.1422	205.51	3.6194	0.1422
New EGR	204.18	3.3751	0.1261	204.13	3.5055	0.1256
% Reduction	0.65%	6.75%	11.30%	0.67%	3.15%	11.64%

It is important to note that the EGR cooler proposed in this study incorporates an individual cooling circuit, the effect of which has not been considered in the analysis. It is expected that this additional cooling circuit, with its associated cooling-pump requirement,

may slightly increase the specific fuel consumption (SFC) compared to the baseline configuration. Moreover, the second low-temperature cooling circuit will result in additional work in packaging and may result in engine reliability issues. Nonetheless, as the primary objective of this study is to reduce emissions, the current results indicate that the new MHE design shows promise in achieving significant reductions in emissions.

4. Conclusions

The primary objective of this study is to assess the feasibility of utilizing a high-efficiency compact microchannel heat exchanger (MHE) as an exhaust gas recirculation (EGR) cooler to reduce emissions from a heavy-duty diesel engine, ultimately aiming to meet stringent EURO 7 regulations. One notable and innovative aspect of this study is the comprehensive explanation of the MHE sizing process, setting it apart from previous studies in the field. In this study, detailed mathematical models for the mechanical and thermal-hydraulic design of an MHE were developed. Additionally, the diesel engine under consideration was modeled using Diesel-RK software to evaluate its performance and calculate emissions. The results show that an MHE with proper design leads to a higher heat-transfer rate, higher effectiveness, and reasonable pressure drop in a much smaller volume compared to the current shell-and-tube design EGR coolers. Furthermore, by implementing the newly designed MHE, it is possible to achieve a reduction in NO_x emissions by 6.75% and PM emissions by 11.30% and a decrease in specific fuel consumption by 0.65% at the analyzed rated power operating point. The results are satisfactory considering the roadmap for reducing NO_x and PM emissions to achieve the Euro 7 diesel emission regulations. The authors intend to analyze the impact of the additional cooling circuit, which is necessary for the newly designed EGR, on the engine efficiency in future research.

Author Contributions: M.O. conducted the ICE modeling and E.G. performed EGR cooler mechanical and thermal-hydraulic analysis. All authors have read and agreed to the published version of the manuscript.

Funding: The Article Processing Charge was funded by the American University of the Middle East, Kuwait.

Institutional Review Board Statement: Not applicable.

Informed Consent Statement: Not applicable.

Data Availability Statement: For the experimental results of this manuscript, you can contact the corresponding author.

Conflicts of Interest: The authors declare no conflict of interest.

References

1. Yusuf, A.A.; Inambao, F.L.; Ampah, J.D. The effect of biodiesel and CeO₂ nanoparticle blends on CRDI diesel engine: A special focus on combustion, particle number, PM_{2.5} species, organic compound and gaseous emissions. *J. King Saud Univ. Eng. Sci.* **2022**, *in press*. [[CrossRef](#)]
2. Yusuf, A.A.; Ampah, J.D.; Veza, I.; Atabani, A.E.; Hoang, A.T.; Nippae, A.; Powoe, M.T.; Afrane, S.; Yusuf, D.A.; Yahuza, I. Investigating the influence of plastic waste oils and acetone blends on diesel engine combustion, pollutants, morphological and size particles: Dehalogenation and catalytic pyrolysis of plastic waste. *Energy Convers. Manag.* **2023**, *291*, 117312. [[CrossRef](#)]
3. News: European Commission proposes Euro 7/VII Emission Standards. Available online: <https://dieselnet.com/news/2022/11eu.php> (accessed on 4 March 2023).
4. Sindhu, R.; Rao, G.A.P.; Murthy, K.M. Effective reduction of NO_x emissions from diesel engine using split injections. *Alex. Eng. J.* **2018**, *57*, 1379–1392. [[CrossRef](#)]
5. Heywood, J.B. *Internal Combustion Engine Fundamentals*; McGraw-Hill Education: New York, NY, USA, 2018. Available online: <https://www.accessengineeringlibrary.com/content/book/9781260116106> (accessed on 8 March 2023).
6. Agrawal, A.K.; Singh, S.K.; Sinha, S.; Shukla, M.K. Effect of EGR on the exhaust gas temperature and exhaust opacity in compression ignition engines. *Sadhana* **2004**, *29*, 275–284. [[CrossRef](#)]
7. Raouf, E.A.; Abdalla, K. N An investigation of some combustion characteristics of turbocharged diesel engines with exhaust gas recirculation. *NVEO Nat. Volatiles Essent. Oils J.* **2022**, *9*, 940–950.

8. Razmavar, A.; Malayeri, M.R.; Abd-Elhady, M.S. Influence of secondary flow on the thermal performance of exhaust gas recirculation (EGR) coolers. *Int. J. Therm. Sci.* **2021**, *161*, 06720. [[CrossRef](#)]
9. Wijeyakulasuriya, S.; Kim, J.; Probst, D.; Srivastava, K.; Yang, P.; Scarcelli, R.; Senecal, P.K. Enabling Powertrain Technologies for Euro 7/VII Vehicles with Computational Fluid Dynamics. *Transp. Eng.* **2022**, *9*, 100127. [[CrossRef](#)]
10. Demirkesen, C.; Zeren, H.B.; Guryuva, S.; Savci, I.H. Numerical and experimental investigation of heavy-duty EGR cooler thermal performance. *Appl. Therm. Eng.* **2022**, *212*, 118531. [[CrossRef](#)]
11. Hooman, K.; Malayeri, M.R. Metal Foams as Gas Coolers for Exhaust Gas Recirculation Systems Subjected to Particulate Fouling. *Energy Convers. Manag.* **2016**, *117*, 475–481. [[CrossRef](#)]
12. Pourrezaei, M.H.; Malayeri, M.R.; Hooman, K. Thermal performance and mechanisms of soot deposition in foam structured exhaust gas recirculation coolers. *Int. J. Therm. Sci.* **2019**, *146*, 106108. [[CrossRef](#)]
13. Han, Z.; Yao, Y.; Tian, W.; Wu, X.; He, G.; Xia, Q. Effect of hydrocarbon condensation on fouling and heat exchange efficiency in EGR cooler. *Int. J. Therm. Sci.* **2023**, *184*, 107898. [[CrossRef](#)]
14. Paz, C.; Suárez, E.; Vence, J.; Hoard, J. Evolution of EGR cooler deposits under hydrocarbon condensation: Analysis of local thickness, roughness, and fouling layer density. *Int. J. Therm. Sci.* **2021**, *161*, 106744. [[CrossRef](#)]
15. Shaik, A.; Vijaya, K.; Reddy, K. Experimental Validation and Combustion Chamber Geometry Optimization of Diesel Engine by Using Diesel-RK. *J. Impact Factor* **2015**, *6*, 92–98.
16. Kamel, M.A.; Abdelaal, M.M.; Rabee, B.A. Improving the performance and emissions of a four-stroke, water-cooled, di diesel engine by increasing inlet air temperature. *J. Al-Azhar Univ. Eng. Sect.* **2022**, *17*, 257–274. [[CrossRef](#)]
17. Kuleshov, A.S. *Multi-Zone DI Diesel Spray Combustion Model and Its Application for Matching the Injector Design with Piston Bowl Shape*; SAE International: Warrendale, PA, USA, 2007. [[CrossRef](#)]
18. Muric, K. Modeling of NOx Formation in Heavy Duty Engines. Master's Thesis, Lund University, Lund, Sweden, 2011.
19. Otkur, M. Altitude Performance and Fuel Consumption Modelling of Aircraft Piston Engine Rotax 912 S/ULS. *J. Adv. Res. Appl. Sci. Eng. Technol.* **2021**, *23*, 18–25. [[CrossRef](#)]
20. Hesselgreaves, J.E. *Compact Heat Exchangers: Selection, Design, and Operation*, 2nd ed.; Elsevier: Amsterdam, The Netherlands, 2017.
21. Mavridou, S.; Mavropoulos, G.C.; Bouris, D.; Hountalas, D.T.; Bergeles, G. Comparative design study of a diesel exhaust gas heat exchanger for truck applications with conventional and state of the art heat transfer enhancements. *Appl. Therm. Eng.* **2010**, *30*, 935–947. [[CrossRef](#)]
22. Shi, X.; Che, D.; Agnew, B.; Gao, J. An investigation of the performance of compact heat exchanger for latent heat recovery from exhaust flue gases. *Int. J. Heat Mass Transf.* **2011**, *54*, 606–615. [[CrossRef](#)]
23. Alcan, G.; Unel, M.; Aran, V.; Yilmaz, M.; Gurel, C.; Koprubasi, K. Predicting NOx emissions in diesel engines via sigmoid NARX models using a new experiment design for combustion identification. *Measurement* **2019**, *137*, 71–81. [[CrossRef](#)]
24. DIESEL-RK. Diesel-RK Is an Engine Simulation Tool. Available online: <https://diesel-rk.com/Eng/> (accessed on 9 July 2023).
25. Kuleshov, A.S. *Model for Predicting Air-Fuel Mixing, Combustion and Emissions in DI Diesel Engines over Whole Operating Range*; Technical Report Number 2005-01-2119; SAE International: Warrendale, PA, USA, 2005. [[CrossRef](#)]
26. ASME BPVC Section VIII-1_2015.pdf. Available online: https://tajhizkala.ir/doc/ASME/ASME%20BPVC%20Section%20VIII-1_2015.pdf (accessed on 22 June 2023).
27. Nellis, G.; Klein, S.A. *Heat Transfer*; Cambridge University Press: Cambridge, UK; New York, NY, USA, 2009.
28. Çengel, Y.A.; Ghajar, A.J. *Heat and Mass Transfer: Fundamentals & Applications*, 5th ed.; McGraw Hill Education: New York, NY, USA, 2015.
29. Shah, R.K.; London, A.L. *Laminar Flow Forced Convection in Ducts: A Source Book for Compact Heat Exchanger Analytical Data*; Academic Press: New York, NY, USA, 1978.
30. Gnielinski, V. Neue Gleichungen für den Wärme- und den Stoffübergang in turbulent durchströmten Rohren und Kanälen. *Forsch. Ingenieurwesen* **1975**, *41*, 8–16. [[CrossRef](#)]
31. Zigrang, D.J.; Sylvester, N.D. Explicit approximations to the solution of Colebrook's friction factor equation. *AIChE J.* **1982**, *28*, 514–515. [[CrossRef](#)]

Disclaimer/Publisher's Note: The statements, opinions and data contained in all publications are solely those of the individual author(s) and contributor(s) and not of MDPI and/or the editor(s). MDPI and/or the editor(s) disclaim responsibility for any injury to people or property resulting from any ideas, methods, instructions or products referred to in the content.